Temperature-dependent structural study of microporous $CsAlSi_5O_{12}$

Martin Fisch[a], Thomas Armbruster[a],*, Boris Kolesov[b]

[a]*Mineralogical Crystallography, Institute of Geological Sciences, University of Bern, Freiestrasse 3, CH-3012 Bern, Switzerland*
[b]*Institute of Inorganic Chemistry at the Russian Academy of Sciences, Novosibirsk, Russia*

Abstract

$CsAlSi_5O_{12}$ crystals were synthesized at high temperature by slow cooling of a vanadium oxide flux. Single-crystal X-ray diffraction structure analysis and electron microprobe analyses yielded the microporous CAS zeolite framework structure of $Cs_{0.85}Al_{0.85}Si_{5.15}O_{12}$ composition. High-temperature single-crystal and powder X-ray diffraction studies were utilized to analyze anisotropic thermal expansion. Rietveld refined cell constants from powder diffraction data, measured in steps of 25 °C up to 700 °C, show a significant decrease in expansion above 500 °C. At 500 °C, a displacive, static disorder–dynamic disorder-type phase transition from the acentric low-temperature space group $Ama2$ to centrosymmetric $Amam$ ($Cmcm$ in standard setting) was found. Thermal expansion below the phase transition is governed by rigid-body TO_4 rotations accompanied by stretching of T–O–T angles. Above the phase transition at 500 °C all atoms, except one oxygen (O6), are fixed on mirror planes. Temperature-dependent polarized Raman single-crystal spectra between −270 and 300 °C and unpolarized spectra between room temperature and 1000 °C become increasingly less resolved with rising temperature confirming the disordered static–disordered dynamic type of the phase transition.
© 2007 Elsevier Inc. All rights reserved.

1. Introduction

Microporous, orthorhombic $CsAlSi_5O_{12}$ (crystallographic data in Table 1) was originally discovered as a byproduct in a study on synthesis of feldspar-type crystals [1]. The crystal structure of $CsAlSi_5O_{12}$ [2] was later assigned to the CAS tetrahedral framework [3]. More recently, a powder neutron diffraction study was performed on $CsAlSi_5O_{12}$ [4] suggesting a partly ordered distribution of Al and Si in the tetrahedral framework: The Si/Al ratio in one tetrahedron is postulated to be 1/1 whereas the remaining two tetrahedra are occupied by Si only.

The CAS framework of $CsAlSi_5O_{12}$ and the BIK framework [3] of the mineral bikitaite $Li_2[Al_2Si_4O_{12}] \cdot 2H_2O$ [5,6] are constructed by the same principles: condensation of five-membered rings of tetrahedra [2] resulting in different topology (CAS and BIK, respec-

tively). $Cs_{0.35}Al_{0.35}Si_{2.65}O_6$ with the BIK tetrahedral framework (Table 1) has been synthesized under hydrothermal conditions and structurally investigated [7]. Cs in $Cs_{0.35}Al_{0.35}Si_{2.65}O_6$ randomly occupies positions, which are completely filled by H_2O in bikitaite *sensu strictu*.

Known Cs framework alumosilicates (Table 1) in addition to $CsAlSi_5O_{12}$ (CAS) are pollucite $CsAlSi_2O_6$ (ANA) [8], $Cs_{0.35}Al_{0.35}Si_{2.65}O_6$ (BIK) [7], and $CsAlSiO_4$ (ABW) [9]. $CsAlSiO_4$ (ABW) transforms to an ANA framework at 1150 °C [10]. This low-ANA framework further transforms upon heating to a cubic high-ANA structure. The low thermal expansion of pollucite, $CsAlSi_2O_6$ (ANA) suggested application in sintered or glass-ceramic bodies [11]. Subsequently, the unusual slope of thermal expansion for pollucite initiated structural analysis [12] between room temperature and 1200 °C. In addition, there are several natural and synthetic zeolites, which were subsequently Cs-exchanged (e.g., LTA, HEU, MOR, MFI, RHO) but these zeolites were not *ab initio* grown as Cs-alumosilicates.

The major interest in crystalline phases in the system $Cs_2O–Al_2O_3–SiO_2$ originated from their possible application

*Corresponding author. Fax: +41 31 631 3996.
E-mail address: armbruster@krist.unibe.ch (T. Armbruster).

Table 1
Cs-framework alumosilicates synthesized in the system $Cs_2O–Al_2O_3–SiO_2$

Formula	Crystal system	Space group	IZA code	a (Å)	b (Å)	c (Å)	Vol. (Å^3)	Z	Ref.
$CsAlSi_5O_{12}$	Orthorhombic	*Ama*2	CAS	16.727(1)	13.785(1)	5.0130(5)	1155.9	2	[1]
$Cs_{0.35}Al_{0.35}Si_{2.65}O_6$	Monoclinic, β: 90.778(9)	*B*2$_1$	BIK	7.3585(4)	5.0334(3)	15.950(1)	590.7	4	[7]
$CsAlSi_2O_6$	Cubic	*Ia3d*	ANA	13.682(3)			2561.2	16	[8]
$CsAlSiO_4$	Orthorhombic	*Pc2$_1$n*	ABW	9.44(3)	5.43(5)	8.89(2)	455.7	4	[9]
$CsAlSiO_4$	Cubic	*Ia3d*	ANA	13.647(3)			2452	24	[10]

as hosts for ^{137}Cs immobilization in radioactive waste management. In this context, a series of papers aimed at studying the stability, solubility, and acid resistance of $CsAlSi_5O_{12}$ and also at studying chemically related compounds for storage of radioactive waste [13–19]. As model system for processing liquid nuclear waste, the zeolite mordenite was saturated with Cs and transformed at 1200 °C to $CsAlSi_5O_{12}$ [10,20]. The leaching rate of Cs from the calcined zeolite transformation products at 1200 °C was three orders of magnitude lower than the leaching rate of Cs from boro-silicate glass.

Bubnova et al. [21] synthesized $CsBSi_5O_{12}$ (orthorhombic, space group *Ama*2, $a = 16.242(4)$ Å, $b = 13.360(4)$ Å, $c = 4.874(1)$), which was found to be isotypic with $CsAlSi_5O_{12}$ (CAS). The material was obtained by heat treatment of boropollucite. The CAS structure type is also found for silica zeolite EU-20b [22] and surprisingly for $EuGa_{2\pm x}Ge_{4\pm x}$, an alloy-like gallium–germanium framework with Eu in the structural channels [23].

In this study, we analyze the thermal behavior of $CsAlSi_5O_{12}$ (CAS) to monitor Cs mobility within the one-dimensional structural channels and to study structural distortion or relaxation accompanied by thermal expansion. Initially, we expected $CsAlSi_5O_{12}$ to show ion conductivity of Cs at elevated temperature, which, however, could not be verified below 700 °C. Instead, we found unusual thermal expansion behavior explained by a displacive order–disorder phase transition.

2. Experimental

2.1. Synthesis and material characterization

Single crystals of $CsAlSi_5O_{12}$ were grown by slow cooling of the title compound in a $BaO–V_2O_5$ flux from 1420 to 750 °C [1]. Elongate (up to few mm), platy (ca. 0.10×0.05 mm^2) crystals were separated from the flux by rinsing with hot NaOH solution. Crystal composition was analyzed with a Jeol JX-8200 electron microprobe, using synthetic $CsVO_3$, natural $Ba(SO_4)$, $K(AlSi_3O_8)$, and $Ca(Al_2Si_2O_8)$ as internal standards. The average crystal composition was $Cs_{0.85}Al_{0.85}Si_{5.15}O_{12}$ with a significant trend of zoning in Cs content ($\pm 5\%$). Deviation from ideal $CsAlSi_5O_{12}$ composition is in accordance with previous findings [1,2]. Portions of the transparent crystals with yellowish hue were ground to a fine powder. Differential thermo-analysis of 7.5 mg of CAS powder between 25 and

700 °C did not show any endo- or exothermic peak. However, a minor change (relative to Al_2O_3 reference material) was observed in the slope of thermal behavior above 500 °C.

2.2. Temperature-dependent experimental methods

2.2.1. X-ray diffraction

Diffraction experiments were performed with an Enraf Nonius CAD4 single-crystal diffractometer (graphite monochromatized Mo$K\alpha$ X-radiation) at room temperature and with a Siemens CCD 1K three-circle SMART diffractometer (graphite monochromatized Mo$K\alpha$ X-radiation) for measurements at 100, 200, 300, 400, 480, 560, 580 and 600 °C. The crystal was mounted on the tip of a SiO_2 glass capillary using ceramic cement. At elevated temperature the crystal was heated using a self-designed, temperature-regulated hot-air blower placed below the goniometer head. Temperature accuracy for this setup was tested to be ± 15 °C at 600 °C. The collected data were reduced and background corrected using either SDP [24] or Saint [25] software. Anisotropic absorption was corrected by multiple psi-scans (CAD4 data) or by pseudo psi-scans of redundant or symmetry equivalent reflections (SMART data). Structure refinement with starting values in space group *Ama*2 [2] was done using the program ShelXTL [26] using neutral atom scattering factors. R_{int} was 2.3% for the room temperature experiment and increased to 7.3% for the measurement at 600 °C (Tables 2 and 3). Due to high-crystal quality with low mosaicity, diffraction data strongly suffered from extinction phenomena and related evidence of multiple diffraction. The refined extinction parameter was 0.040(2) for the room temperature measurement and decreased with increasing temperature to 0.009(2) at 600 °C. The value of extinction could have been reduced by choosing a smaller crystal. However, X-ray diffraction (XRD) intensities strongly decrease with rising temperature. Thus, the relatively large crystal size was necessary for the high-temperature experiments. Refined parameters were atomic coordinates, occupancy of Cs, anisotropic displacement parameters for all atoms, extinction, and twinning by the inversion operation. Data collection and refinement parameters for the ambient and high-temperature experiments are shown in Tables 2 and 3, respectively.

Powder XRD measurements were made on a PANalytical X'Pert Pro MPD θ–θ diffractometer using Ni-filtered 1.6 kW Cu$K\alpha$ radiation. The beam path included a 0.25°

Table 2
Parameters for X-ray data collection and crystal structure refinement at room temperature

Diffractometer	Enraf Nonius CAD4
X-ray radiation	MoKα (0.71073 Å)
X-ray power	50 kV, 40 mA
Crystal size	$0.4 \times 0.2 \times 0.1$ mm^3
Time per scan	Max. 120 s
Absorption correction	Empirical, psi-correction
Temperature	25 °C
Space group	*Ama*2
a-axis length	16.7234(12) Å
b-axis length	13.7779(11) Å
c-axis length	5.0075(6) Å
Cell volume	1153.79(19) Å
Z	2
Reflections collected	3767
Max. 2θ	80.21°
Index range *h*	−1 to 30
Index range *k*	−1 to 24
Index range *l*	−5 to 9
Unique reflections	3315
Reflections $>2\sigma(I)$	2722
R(int)	0.0231
R(σ)	0.0181
L.S. parameter no.	93
GOF	1.057
*R*1, $I>2\sigma(I)$	0.0462
*R*1, all data	0.0597
w*R*2 (on F^2)	0.1360
$\Delta\rho_{min}$ (eÅ^{-3}) close to Cs	−1.04
$\Delta\rho_{max}$ (eÅ^{-3}) close to Cs	1.83

antiscatter slit and a 0.125° divergence slit in the primary path and a 0.125° antiscatter slit in the diffracted beam. The X'Celerator detector was set to scanning mode with a sensitive area of 2.122° resulting in a step-size of 0.008°/step and a measurement time of 70 s/step. Sample rotation was 30 rpm. The diffractometer was equipped with an Anton Paar HTK1200 heating-chamber and measurements were made from 25 to 700 °C in steps of 25 °C. Powder diffraction data were recorded from 10° 2θ to 75° 2θ and Rietveld refined using FullProf 2000 [27].

2.2.2. Raman spectroscopy

All Raman spectra were measured from −270 to 1000 °C on a $CsAlSi_5O_{12}$ single crystal using a Triplemate, SPEX, triple-grating spectrometer with CCD detector, model LN-1340 PB, from Princeton Instruments. The 514 nm line of an Ar^+ laser was used for the spectral excitation. The diameter of the laser spot on the sample surface was 1–2 μm. The laser power at the sample was typically 5–10 mW. The low- and room temperature spectra were measured in 180° collection geometry with a microscope. Low-temperature spectra were recorded by mounting the crystal on a cold finger of a helium cryostat. The precision of the measured temperatures is estimated to be ±1 °C. All measurements were performed with a spectral resolution of 2 cm^{-1}.

3. Results

3.1. Powder diffraction

Precise cell constants were refined from powder diffraction data in *Ama*2 setting (Fig. 1). The change in gradient of the axial and volume evolution with temperature suggested a phase transition at about 500 °C. As will be shown below, high-temperature single-crystal XRD confirmed a displacive phase transition from the acentric space group *Ama*2 (No. 40) to the centrosymmetric space group *Amam* (No. 63, *Cmcm* in standard setting) at 500 °C. The *b*-, *c*-axis and the volume show a distinct decrease in slope at about 500 °C. In contrast, the slope of the *a*-axis remains more or less uninfluenced below and above the phase transition at 500 °C. Between 25 and 300 °C the temperature-dependent evolution of the *a*- and *b*-axis is different. The *a*-axis starts with a steep gradient, which levels off towards higher temperature, whereas the gradient of the *b*-axis starts small and increases with rising temperature. The different curvatures of the *a*- and *b*-axis in the range from 25 to 300 °C seem to compensate each other, such that the volume exhibits nearly linear behavior below and above 500 °C. Between 300 and 500 °C, both gradients (*a*, *b*) behave almost linear. temperature-dependent cell dimensions and quality parameters of the corresponding Rietveld refinements are given in Appendix A.

In addition, thermal expansion coefficients α ($\alpha = f^{-1} \times f'$, where *f* is a function expressing temperature dependence of cell dimensions and f' is its first derivative) have been calculated (Fig. 2) by fitting temperature-dependent unit cell data with a third-order polynomial. Data above and below the phase transition were treated separately.

3.2. Single-crystal diffraction

The structure refinements of the single-crystal data showed that with rising temperature correlations between oxygen atoms O6A and O6B continuously increased. Above the phase transition at 500 °C, they are no longer symmetrically independent but become related by a mirror plane. The exact temperature of the displacive transition was taken from the temperature dependence of cell dimensions (powder data). The centrosymmetric space group was recognized due to the appearance of new mirror planes parallel to (001) at $z = 0$ and 0.5 in *Ama*2. If the axial orientation is maintained, the high-temperature space group is *Amam* corresponding to *Cmcm* in standard setting (interchange of *a*- and *c*-axis). Thus the new mirror planes in *Cmcm* setting are parallel to (100) at $x = 0$ and 0.5. Atomic coordinates and isotropic displacement parameters for the temperature-dependent measurements and corresponding anisotropic displacement factors are summarized in Appendix A.

Above 500 °C, in space group *Cmcm*, O6A and O6B are located at symmetry equivalent positions and are therefore

M. Fisch et al. / Journal of Solid State Chemistry 181 (2008) 423–431

Table 3
Parameters for X-ray data collection and crystal structure refinement from 100 to 600 °C

Diffractometer	Siemens Smart CCD 1K
X-ray rad.	MoKα (0.71073 Å)
X-ray power	50 kV, 40 mA
Crystal size	$0.4 \times 0.2 \times 0.1$ mm^3
Detector dist.	5.4 cm
Rotation axis	Omega
Rot. width	0.3°
Coll. Mode	Automated hemisphere
No. of frames	1362
Frame size	512×512 pixel
Time p. frame	10 s
Abs. corr.	Empirical, pseudo-psi correction

| Temperature	100 °C	200 °C	300 °C	400 °C	480 °C	560 °C	580 °C	600 °C
Space group	*Ama*2	*Ama*2	*Ama*2	*Ama*2	*Ama*2	*Cmcm*	*Cmcm*	*Cmcm*
a-axis (Å)	16.744(3)	16.766(3)	16.777(3)	16.786(4)	16.799(4)	5.1147(12)	5.1171(10)	5.1182(10)
b-axis (Å)	13.788(3)	13.799(3)	13.811(3)	13.839(3)	13.864(3)	13.884(3)	13.881(3)	13.884(3)
c-axis (Å)	5.0269(10)	5.0466(10)	5.0652(10)	5.0859(13)	5.1043(12)	16.814(4)	16.816(3)	16.820(3)
Volume (Å^3)	1160.5(4)	1167.6(4)	1173.6(4)	1181.5(5)	1188.8(5)	1194.0(5)	1194.5(4)	1195.2(4)
Z	2	2	2	2	2	2	2	2
Refl. coll.	2546	2568	2580	2605	2621	1569	2626	2654
Max. 2θ (°)	55.46	55.37	55.28	55.45	55.39	55.33	55.33	55.32
Index range *h*	−21 to 12	−21 to 12	−21 to 13	−13 to 21	−13 to 21	−6 to 4	−6 to 4	−6 to 4
Index range *k*	−16 to 18	−16 to 18	−18 to 16	−18 to 16	−18 to 16	−15 to 18	−18 to 16	−18 to 16
Index range *l*	−6 to 4	−6 to 4	−4 to 6	−6 to 4	−6 to 4	−13 to 20	−21 to 13	−21 to 13
Unique refl.	1052	1061	1064	1078	1085	634	761	768
Refl. $>2\sigma(I)$	951	943	915	900	855	414	557	554
R(int)	0.0603	0.0593	0.0610	0.0605	0.0669	0.1735	0.0713	0.0737
$R(\sigma)$	0.0450	0.0448	0.0466	0.0461	0.0517	0.0910	0.0480	0.0508
L.S. param.	92	92	92	92	92	60	60	60
GOF	1.086	1.095	1.110	1.055	1.125	1.053	1.118	1.131
$R1$, $I>2\sigma(I)$	0.0409	0.0456	0.0486	0.0550	0.0603	0.0712	0.0632	0.0644
$R1$, all data	0.0445	0.0510	0.0550	0.0630	0.0715	0.0991	0.0822	0.0829
w$R2$ (on F^2)	0.1104	0.1245	0.1370	0.1543	0.1789	0.2206	0.1959	0.2001
$\Delta\rho_{min}$ (eÅ^{-3})[a]	−0.58	−0.63	−0.58	−0.52	−0.6	−0.90	−0.69	−0.71
$\Delta\rho_{max}$ (eÅ^{-3})[a]	0.75	0.67	0.71	0.82	0.87	0.99	1.07	1.03

[a] Close to Cs.
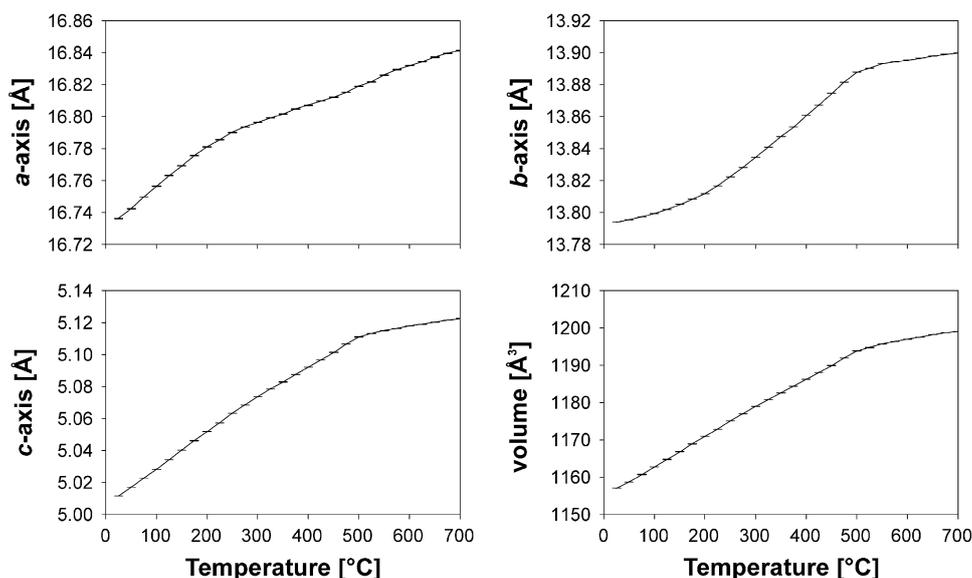
Fig. 1. Evolution of the *a*-, *b*- and *c*-axis and the cell volume with temperature. Cell dimensions from 25 to 500 °C are given in *Ama*2 setting and from 500 to 700 °C in *Amam* setting (instead of standard *Cmcm*) for better comparison.
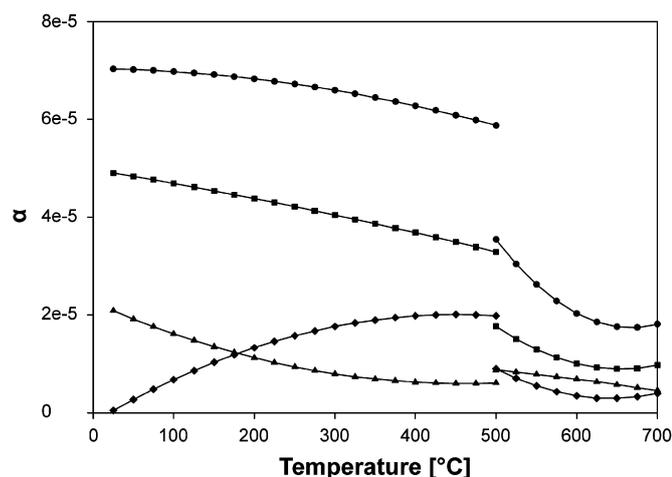
Fig. 2. Plot of the polynomials expressing the thermal expansion coefficients α of $CsAlSi_5O_{12}$. α is calculated as $\alpha = f^{-1} \times f'$, where f is a function expressing temperature dependence of cell dimensions and f' is its first derivative. The expansion coefficient for the a-axis is plotted as triangles, for the b-axis as diamonds, for the c-axis as squares and for the volume as circles. Axial orientation from 25 to 500 °C is given in *Ama*2 setting and from 500 to 700 °C in *Amam* setting (instead of standard *Cmcm*) for better comparison.
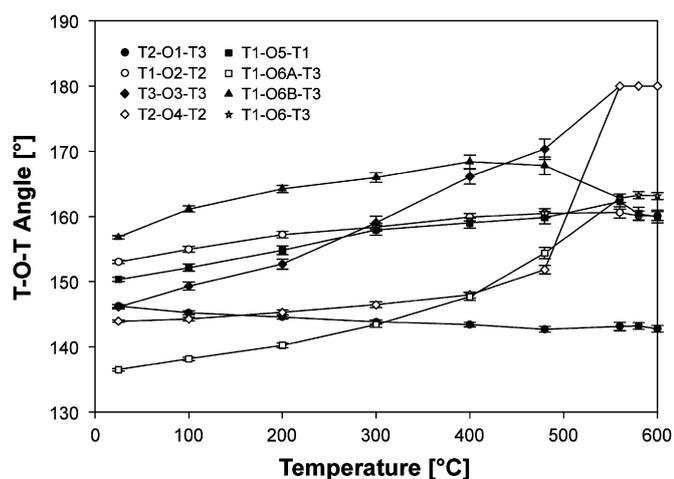

Fig. 4. Mean Cs–O bond distance evolution with increasing temperature.

Fig. 3. Temperature dependence of inter-tetrahedral T–O–T angles: above the phase transition, O6A and O6B are equivalent to O6.

Fig. 5. Mean T–O bond distance evolution with temperature. T1–O lengths are marked with triangles, T2–O lengths with circles and T3–O lengths with squares. Uncorrected values from single crystal X-ray data are plotted as solid lines, data corrected according to the "riding model" [31] are plotted as dashed lines.

named O6. The temperature dependence of T–O–T inter-tetrahedral angles and Cs-O bond lengths is shown in Figs. 3 and 4. Due to the flexibility of the tetrahedral framework with temperature, the number (between 12 and 16) and type of oxygen atoms from the framework contributing to the average Cs–O bond length varied. All Cs-O distances below the shortest Cs–Si distance were considered (Appendix A). Bond lengths from the central atom of a tetrahedron to its ligands (T–O bond lengths) are shown in Fig. 5.

3.3. Raman spectroscopy

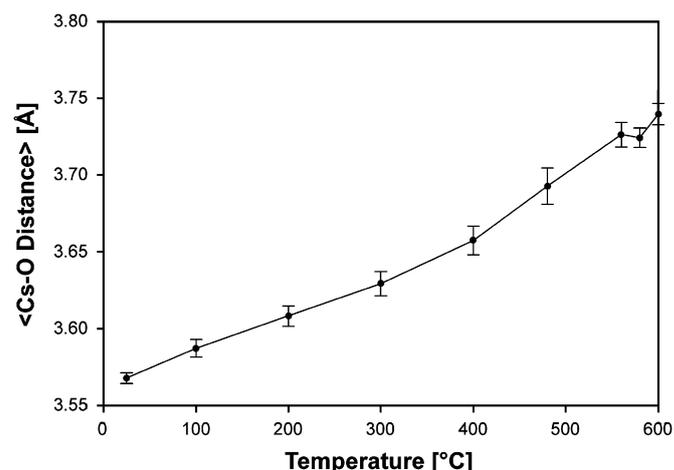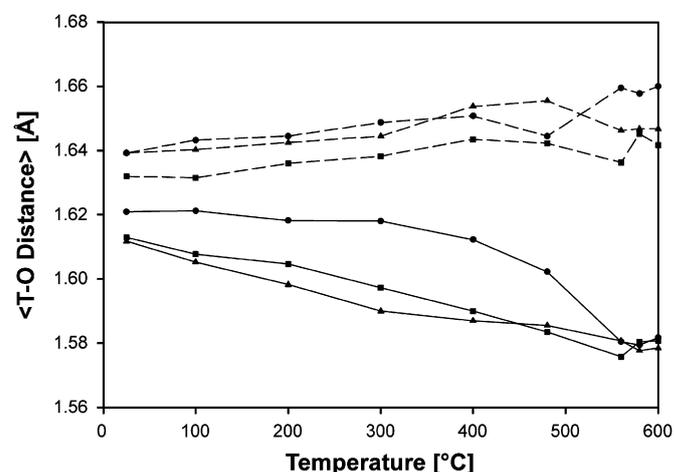Based on structural data, a symmetry analysis of the $CsAlSi_5O_{12}$ vibration spectrum can be carried out. There

are no isolated $(Si,Al)O_4$ tetrahedra in the lattice; therefore, the analysis involves only translational motions of all atoms, i.e. Cs, Al, Si, and O. Resulted motions of Al, Si, and O give the vibrational modes that should be similar to external (translational and librational) and internal (bending and stretching) modes of the tetrahedra. Vibrations of Cs have quite definite meaning of translations along all three axes in the cavity.

All modes are Raman active (Table 4). Polarized Raman spectra at −270 and 27 °C are shown in Figs. 6a and b. All observed bands are broadened at both low and ambient temperature. The broadening may be caused by some lattice disorder or the presence of several overlapping modes with close frequencies for each spectral position or both. The low-intensity modes in the range of 750–950 cm^{-1} are attributed to stretching vibrations of the tetrahedra. The bands at 400–500 cm^{-1} are assigned to bending modes of the tetrahedra. Those at 300–350 and

Table 4
Active Raman modes

$Ama2$ (C_{2v}^{16})	O_1 (C_2)	Cs, O_2 (C_{1h})	Si, Al, O3–O7 (C_1)
A_1	z	y, z	x, y, z
A_2	z	x	x, y, z
B_1	x, y	x	x, y, z
B_2	x, y	y, z	x, y, z

Fig. 6. Polarized Raman spectra of oriented CsAlSi$_5$O$_{12}$-crystals at $-270\,°C$ (a) and $27\,°C$ (b). *ab*-Raman spectra at different temperature are shown in (c) for -270 to $27\,°C$ and in (d) for 20–$1000\,°C$. The change in spectrum indicating the phase transition is marked with an arrow (d). The spectrum at room temperature after heating is shown by the dotted curve (d).

temperature. The frequency of Cs-related mode changes very slightly from $93\,cm^{-1}$ at $-270\,°C$ to $92\,cm^{-1}$ at room temperature. At high temperature (Fig. 6d), the spectra show considerable changes around $500\,°C$ (they become simpler and less resolved) confirming the presence of the phase transition observed in structural measurements. However, the mode of Cs-vibrations remains invariable at all temperatures.

4. Discussion

When viewed along the *c*-axis in the setting of space group *Ama*2, the CAS framework structure [2,3] is built of two types of rings, one consisting of eight O atoms and the other consisting of five O atoms. Parallel to the *c*-axis, voids within the eight-membered rings form large tunnels, whereas the channels through the five-membered rings are much narrower and not permeable for alkaline or earth alkaline cations (Fig. 7). In projections along the *b*-axis, the Cs atom occupies an extraframework position between two stacked (parallel to *c*) eight-membered rings. Projected along the *c*-axis, the Cs atom is slightly displaced from the ring center. Cs–O bond distances at room temperature (Appendix A) are similar to the ones reported by Araki [2]. Parallel to *b*, eight-membered rings are connected by bowties formed by symmetry equivalent (Si,Al)O$_4$-tetrahedra (T1). Adjacent eight-membered rings are separated along *a* by a chain of five-membered rings extending parallel to the *b*-axis [2].

When the structure of CsAlSi$_5$O$_{12}$ is projected along the *b*-axis, it becomes obvious that the tetrahedra forming the eight-membered rings do not lie in a plane. They are bent around the Cs atom, and the T1 bowties connecting two
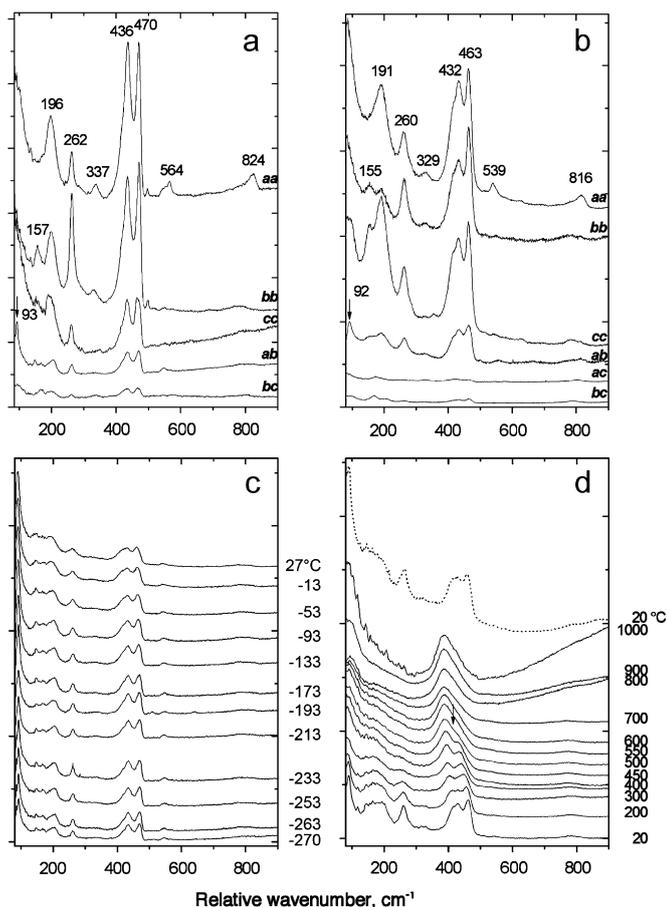
150–$300\,cm^{-1}$ are assigned to restricted rotational and translational motions of the tetrahedra, respectively. The lowest frequency band at 92–$93\,cm^{-1}$ is attributed to Cs-motion. This band is most intensive in the *ab*-spectrum (Figs. 6a and b) (i.e. spectrum with polarization of incident laser light directed along *a*-axis and polarization of scattered light directed along *b*-axis of the crystal) where A_2 modes are active relating the motion of extraframework Cs along the *a*-axis of the crystal (Table 4).

Figs. 6c and d show polarized *ab*-Raman spectra versus temperature in the range of -270 to 27 and 20–$1000\,°C$. There is no marked change of the spectra at low
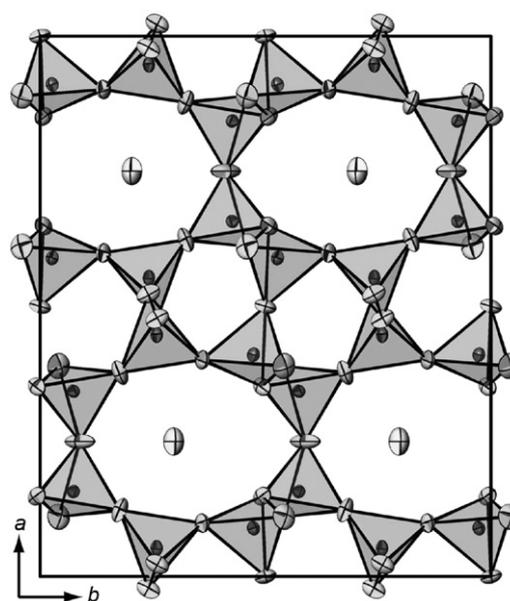

Fig. 7. Unit cell of CsAlSi$_5$O$_{12}$ projected along the *c*-axis at $25\,°C$ showing the five- and eight-membered rings.

eight-membered rings are at different levels along the c-axis (Fig. 8).

The thermal evolution of the structure can be best described in a view parallel to *a* in *Ama*2 setting (Fig. 9). The eight-membered rings around the Cs atom stretch with increasing temperature: the connected tetrahedra T1, T2, T3 approach a common plane perpendicular to *c*. Alternatively, this movement can also be described by tetrahedral rotations around an axis parallel to *a*. In addition, the tetrahedra rotate around an additional axis parallel to *b*. With increasing temperature, the T1 rotation parallel to *b* leads to expansion along the *a*-axis (*Ama*2 setting). The non-uniform increase of the cell dimensions *a* and *b* between 25 and 300 °C (Fig. 1) must be related to the different onsets and magnitudes of the latter types of rotation. These combined tetrahedral rotations increase preferentially the T1–O6A–T3 and the T3–O3–T3 angles until the phase transition occurs. Stretching of the chain T3–T2–T1 increases the *b*-axis. The strongest thermal expansion along *c* (*Ama*2 setting) must be ascribed to the combination of rigid-body-type tetrahedral rotations along axes parallel to *a* and *b* (Figs. 8 and 9).

Above the phase transition at 500 °C, the ring is completely unrolled (the average of the corresponding T–O–T angles T3–O3–T3 and T2–O4–T2 is 180°) and the Cs atom, all Si atoms and all O atoms, except O6, lie on special positions (0, *y*, *z*) (Appendix A). New mirror planes through these positions increase the symmetry to space group no. 63 (*Cmcm*). Due to increase in space group symmetry, O6A and O6B are now at symmetry equivalent positions and are therefore both named O6. The decrease of thermal expansion above 500 °C is readily explained by the fixation of atoms on special positions (mirror planes). Thus, the initial motor of thermal expansion below 500 °C,
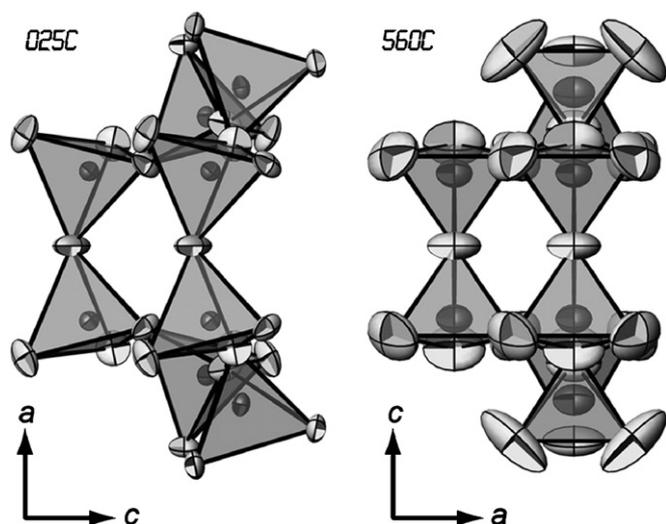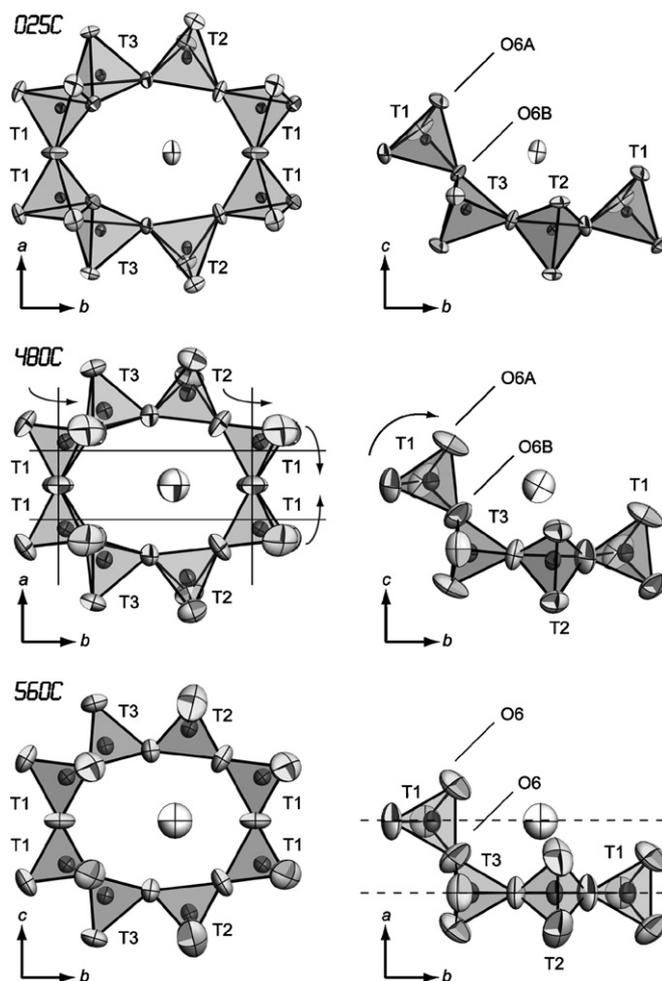

Fig. 9. Two projections of the eight membered rings at different temperatures. Cell settings are *Ama*2 for 25 and 480 °C and *Cmcm* for 560 °C. At 25 °C, the ring is bent around the Cs atom (top left) and O6A and O6B are not on symmetry equivalent positions due to tetrahedral rotation (top right). At 480 °C, just below the phase transition, T1 rotation is illustrated with lines and arrows (middle left). O6A and O6B are almost on equivalent positions and the ring is still slightly bent around the Cs atom (middle right). At 560 °C, above the phase transition, the ring is completely flattened (bottom left) and unrolled. In addition, O6A and O6B are situated on symmetry equivalent positions and are labelled O6. All T atoms lie on special positions with respect to *x*-coordinates, consequently new mirror planes appear (dashed lines, bottom right).

the individual rotation of tetrahedra, is prohibited by increase of symmetry.

At temperatures above 500 °C, atomic vibrations parallel to the channel axis are perpendicular to the mirror plane that is unique to the high-temperature phase. These vibrations may be considered as "up" and "down" with the center of gravity fixed on the mirror plane. Below 500 °C, these time and space disordered "up" and "down" motions freeze on positions displaced from the mirror plane and develop twin domains related by the high-temperature characteristic mirror plane. This explanation also confirms that below 500 °C a CAS crystal is composed of a twin ratio of 1/1 for statistical reasons. Above 500 °C, the framework may be considered dynamically disordered

Fig. 8. Ring consisting of eight (Si,Al)O₄ tetrahedra at 25 °C (left, *Ama*2) and at 560 °C (right, *Cmcm*). The two tetrahedra on the left of each ring are shared by two rings. Stretching of the shortest crystal axis (*c* in *Ama*2 and *a* in *Cmcm*, respectively) is caused by tetrahedral rotation.

because in time and space random domains may develop, which locally resemble the twin individuals of the low-temperature structure. Evidence of the dynamically disordered character is the rapid increase of the displacement parameter of O4 above the phase transition. At low temperature, the framework is statically disordered as indicated by twinning. Crystals of $CsAlSi_5O_{12}$ were grown by slow cooling of a flux to 750 °C. Thus, the starting material of this study is formed in its high-temperature modification and transformed upon cooling to the acentric twinned modification. Absence of endo- or exothermic effects in differential thermal analysis is in agreement with the displacive static to dynamic phase transition and vise versa.

Evidence of the phase transition was also observed in Raman spectra as the spectra showed significant changes above 500 °C (Fig. 6d). In particular, the bands measured at temperatures above the phase transition show less fine structure and the whole spectrum appears simpler as characteristic for a low to high symmetry transition. The same spectra also indicate that there are no other phase transitions at temperatures lower than 500 °C.

Based on a recent powder neutron diffraction study on $Cs_4Al_4Si_{20}O_{48}$, Hughes and Weller [4] suggest that the (Si,Al) distribution on the tetrahedral sites is not at random. Instead, Al is preferably situated on one tetrahedron having a Si/Al ratio of 1/1, while the remaining two tetrahedra are occupied by Si only. In the present study, (Si,Al) order [4] could not be confirmed because bond lengths (Fig. 5) for all three symmetry-independent tetrahedra were found to be rather equal and in addition, difference displacement parameters evaluated along the bonding T–O vector show no supporting evidence for Al order.

In feldspars, the mean T–O distance of Si–O is $\langle 1.61\,\text{Å} \rangle$ and the corresponding value for Al–O is $\langle 1.74\,\text{Å} \rangle$ [28]. Thus, for a Si/Al ratio of 1/1, one should expect an average T–O bond length of $\langle 1.675\,\text{Å} \rangle$, which is in contrast to T2–O [4] with $\langle 1.618\,\text{Å} \rangle$ and the corresponding site T1–O (this study) with $\langle 1.612\,\text{Å} \rangle$. Atom displacement parameters (mean square vibrational amplitudes) parallel to T–O bonds have been calculated from data obtained in this study (Table 5). Difference mean square displacement parameters ($\Delta U = U_O - U_T$) evaluated along the bonding direction within a TO_4 tetrahedron reflect the disorder contribution in atomic displacement parameters due to the size difference of a small SiO_4 (Si–O: $\langle 1.61\,\text{Å} \rangle$) and a larger AlO_4 (Al–O: $\langle 1.74\,\text{Å} \rangle$) tetrahedron, if SiO_4 and AlO_4 are statistically superimposed. Theoretically, a TO_4 tetrahedron occupied to 50% each by Si and Al has a mean T–O distance of $\langle 1.675\,\text{Å} \rangle$ accompanied by $\langle \Delta U = 0.00467\,\text{Å}^2 \rangle$ [28] whereas a TO_4 tetrahedron occupied by 1/6 Al and 5/6 Si (as calculated for a random Al distribution) is predicted to have a mean T–O distance of $\langle 1.632\,\text{Å} \rangle$ with $\langle \Delta U = 0.00279\,\text{Å}^2 \rangle$. In case of our $CsAlSi_5O_{12}$ data neither mean T–O distances nor ΔU values (Table 5) support Al order on one specific tetrahedral site.

Table 5
Mean square vibrational amplitudes calculated parallel to T–O bond direction for 25 °C data

Bond	U_{Si} parallel to bond (Å^2)	U_O parallel to bond (Å^2)	ΔU parallel to bond (Å^2)
T1–O2	0.0169	0.0212	0.0043(13)
T1–O5	0.0185	0.0222	0.0037(12)
T1–O6A	0.0169	0.018	0.0011(15)
T1–O6B	0.0197	0.0221	0.0024(18)
T1–O Average			$\langle 0.0029(15) \rangle$
T2–O1	0.0164	0.0208	0.0044(10)
T2–O2	0.0211	0.0273	0.0062(15)
T2–O4	0.0151	0.0183	0.0032(10)
T2–O4	0.0246	0.0253	0.0007(15)
T2–O Average			$\langle 0.0036(13) \rangle$
T3–O1	0.0168	0.0189	0.0021(9)
T3–O3	0.0216	0.0213	−0.0003(11)
T3–O6A	0.0188	0.0214	0.0026(13)
T3–O6B	0.0193	0.0216	0.0023(12)
T3–O Average			$\langle 0.0017(12) \rangle$

Our temperature-dependent data indicate that tetrahedral rotations play a major role for the interpretation of thermal expansion. Thus, one may suspect that at a given temperature TO_4 units are characterized by strong librational modes as well. Rigid body libration of tetrahedra leads to apparent shortening of T–O distances determined from XRD data [29]. This bond shortening can be corrected by a "riding model" [30] where a ligand atom is so strongly linked to a central atom that it appears to ride. The riding model corrects the bond length by the difference of mean square displacement amplitudes between ligand and central atom evaluated perpendicular to the T–O vector. Uncorrected mean $\langle T-O \rangle$ bond lengths evaluated for $CsAlSi_5O_{12}$ at different temperatures seem to decrease with temperature (Fig. 5). However, this is an artifact due to increasing rigid body libration with rising temperature. If this apparent shortening is corrected by a riding model [31], even T–O distances slightly increase with temperature (Fig. 5). Corrected $\langle T-O \rangle$ bond lengths at room temperature yield $\langle T-O \rangle$ distances between 1.632 and 1.639 Å, which is close to the expected value for a random (Si, Al) distribution within the CAS tetrahedral framework. Furthermore, the rather low-resolution ^{29}Si MAS NMR spectrum presented by Hughes and Weller [4] is—as admitted by the authors—not good enough to provide an independent estimate of (Si, Al) order. These different findings allow two possible interpretations. Either the different synthesis route by Hughes and Weller [4], using a sol–gel method with final sintering at 1200 °C, produced a material with different (Si, Al) order characteristics, or more probably, the suggestion of (Si, Al) order in the CAS framework [4] is based on an artifact due to non-ideal experimental data. The similarity of uncorrected average $\langle T-O \rangle$ distances in our X-ray single-crystal study to those from neutron-powder diffraction results [4] rather suggests an artifact.

5. Conclusions

The initial hypothesis that $CsAlSi_5O_{12}$ may become an ion conductor with increasing temperature could not be confirmed. Cs vibration at elevated temperature remains rather isotropic and no evidence for increased Cs displacement parallel to the channel axis could be found. Below 500 °C the CAS framework expands gradually, controlled by rigid body tetrahedral rotations, until the inter-tetrahedral angles T3–O3–T3 and T2–O4–T2 adopt an average value of 180°. At this stage, the structure changes from acentric to centric. However, T–O–T angles of 180° are known to be energetically unfavorable [32] and must be interpreted as an average of local T–O–T angles smaller and larger than 180°. This disorder is also evident from the rapid increase of the O4 displacement parameters above the phase transition. Under the applied experimental conditions, it is assumed that crystals of the CAS framework originally crystallized at high temperature in the centrosymmetric space group *Cmcm* and transformed upon cooling to acentric crystals of symmetry *Ama*2, which are twinned by mirror planes existing as true symmetry elements in the high-temperature modification.

Acknowledgments

Appendix A. Supplementary materials

Supplementary data associated with this paper can be found in the online verison at doi:10.1016/j.jssc.2007.12.014

Appendix B

Further details of the crystal structure investigations can be obtained from the Fachinformationszentrum Karlsruhe, 76344 Eggenstein-Leopoldshafen, Germany (fax: (49) 7247-808-666; e-mail: crysdata@fiz.karlsruhe.de under depository numbers: CSD-418959 (25 °C), CSD-418958 (100 °C), CSD-418957 (200 °C), CSD-418956 (300 °C), CSD-418955 (400 °C), CSD-418954 (480 °C), 418953 (560 °C), CSD-418952 (580 °C) and CSD-418951 (600 °C).

References

[1] J. Ito, Am. Minerol. 61 (1976) 170–171.
[2] T. Araki, Z. Krist. 152 (1980) 207–213.
[3] C. Bearlocher, W.M. Meier, D.H. Olson, Atlas of Zeolite Framework Types, Elsevier, Amsterdam, 2001, pp. 88–89.
[4] R.W. Hughes, M.T. Weller, Micro. Meso. Mater. 51 (2002) 189–196.
[5] V. Kocman, R.I. Gait, J. Rucklidge, Am. Minerol. 59 (1974) 71–78.
[6] S. Quartieri, A. Sani, G. Vezzalini, E. Galli, E. Fois, A. Gamba, G. Tabacchi, Micro. Meso. Mater. 30 (1999) 77–87.
[7] H. Annehed, L. Fälth, Z. Krist. 166 (1984) 301–306.
[8] R.E. Newnham, Am. Minerol. 52 (1967) 1515–1518.
[9] R. Klaska, Hydrothermalsynthesen und Strukturuntersuchungen zu kationenabhängien Veränderungen von aufgefüllten Tetraedergerüsten aus dem Bereich der Feldspäte und seiner Vertreter, Ph.D. Dissertation, Fachbereich Geowissenschaften, University of Hamburg, Germany, 1970.
[10] R. Dimitrijevic, V. Dondur, N. Petranovic, J. Solid State Chem. 95 (2) (1991) 335–345.
[11] D.W. Richerson, F.A. Hummel, J. Am. Ceram. Soc. 55 (1972) 269–273.
[12] I. Yanase, H. Kobayashi, Y. Shibasaki, T. Mitamura, J. Am. Ceram. Soc. 80 (1997) 2693–2695.
[13] R. Odoj, K. Hilpert, Z. Naturforsch. A: Phys. Sci. 35A (1) (1980) 9–13.
[14] T. Adl, E.R. Vance, J. Mater. Sci. 17 (3) (1982) 849–855.
[15] S. Komarneni, R. Roy, J. Am. Ceram. Soc. 66 (6) (1983) 471–474.
[16] E.R. Vance, F.J. Ahmad, Nucl. Chem. Wasteman. 4 (2) (1983) 171–176.
[17] E.R. Vance, L. Cartz, F.G. Karioris, J. Mater. Sci. 19 (9) (1984) 2943–2947.
[18] P. Taylor, S. DeVaal, D.G. Owen, Can. J. Chem. 67 (1) (1989) 76–81.
[19] H. Mimura, K. Iijima, K. Akiba, J. Nucl. Sci. Technol. 34 (3) (1997) 269–276.
[20] T. Kanno, Nendo Kagaku 25 (1) (1985) 1–10.
[21] R.S. Bubnova, M.G. Krzhizhanovskaya, S.K. Filatov, V.L. Ugolkov, P. Paufler, Z. Krist. 222 (2007) 83–88.
[22] B. Marler, M.A. Camblor, H. Gies, Micro. Meso. Mater. 90 (2006) 87–101.
[23] W. Carillo-Cabrera, S. Paschen, Y. Grin, J. Alloys Compd. 333 (1–2) (2002) 4–12.
[24] Enraf Nonius, Structure Determination Package (SDP), Delft, Netherlands, 1983.
[25] Bruker, SMART and SAINT, Bruker AXS Inc., Madison, Wisconsin, USA, 2001.
[26] G.M. Sheldrick, ShelXTS and ShelXTL, University of Goettingen, Germany, 1997.
[27] J. Rodriguez-Carvajal, FullProf 2000 v. 3.40, Laboratoire Léon Brillouin (CEA-CNRS), Gif-sur-Yvette Cedex, France, 2006.
[28] M. Kunz, T. Armbruster, Am. Minerol. 75 (1990) 141–149.
[29] R.T. Downs, G.V. Gibbs, K.L. Bartelmehs, Am. Minerol. 77 (1992) 751–757.
[30] W.R. Busing, H.A. Levy, Acta Crystallogr. 17 (1964) 142–146.
[31] C.K. Johnson, in: F.R. Ahmed (Ed.), Crystallographic Computing, Munksgaard, Copenhagen, 1970, pp. 220–226.
[32] G.V. Gibbs, Am. Minerol. 67 (1982) 421–450.